Journal of Power Sources 194 (2009) 1061–1067

Contents lists available at ScienceDirect

Journal of Power Sources

journal homepage: www.elsevier.com/locate/jpowsour

Electrochemical properties of negative $SiMo_x$ electrodes deposited on a roughened substrate for rechargeable lithium batteries

Chang-Mook Hwang, Chae-Ho Lim, Jae-Hoon Yang, Jong-Wan Park*

Department of Materials Science and Engineering, FERI, Hanyang University, 17 Haengdang-dong, Seongdong-gu, Seoul 133-791, Republic of Korea

ARTICLE INFO

Article history:
Received 11 February 2009
Received in revised form 20 April 2009
Accepted 28 May 2009
Available online 9 June 2009

Keywords:
Silicon based alloy
Roughened substrate
SiMo
Rechargeable lithium batteries, Negative electrode (anode)

ABSTRACT

To replace conventional carbon, silicon has been widely proposed as a next-generation negative electrode (anode) material for lithium-ion batteries. In this study, Si and $SiMo_x$-alloy deposited by an RF-magnetron sputtering system is investigated by means of X-ray diffraction, ex situ Raman spectroscopy and transmission electron microscopy. Electrochemical tests are conducted and four different Si and $SiMo_x$-alloy electrodes and their structures and textual properties are characterized with X-ray photoelectron spectroscopy. The surface morphologies of the electrodes are also observed using field-emission scanning electron microscopy. The electrochemical properties of the electrodes are examined through cycling tests and electrochemical impedance spectroscopy. The results show that rough Cu foil and Mo as alloy materials help Si to retain its discharge capacity and overcome volume expansion during charging and discharging. After a few cycles, the Si electrode severely loses capacity, whereas the $SiMo_x$-alloy electrodes display good cycle retention and high capacity. The $SiMo_{0.79}$ electrode gives an initial capacity of 1319 mAh g^{-1} that decreases to 1180 mAh g^{-1} after 100 cycles (89.4%).

1. Introduction

Lithium-ion secondary batteries (LIBs) are widely used in various portable electric devices such as laptop computers, cell phones, camcorders, and personal digital appliances. Compared with general-use batteries, the attributes of LIBs are high cell voltage, high specific energy, and high specific capacity [1,2]. The capacity of carbon electrode materials reaches about 350 mAh g^{-1}, which is close to the theoretical value of the carbon intercalation composition LiC_6, and results in a relatively low volumetric lithium capacity. Despite the advantage of carbon, it will not adjust well to the needs of future devices due to its limited capacity (LiC_6). Recently, many research activities have focused on the most important issue in rechargeable Li-ion batteries, namely, the growing demand for high specific energy, long-lasting, compact power sources for portable electronic devices.

Lithium alloys (e.g. Li_xM (M = Sn, Si, Ge, Al)) have attracted attention as alternative negative electrode (anode) materials for LIBs because of their high specific capacities and high packing densities compared with common anode materials [3–5]. Of these alloys, silicon shows the highest specific capacity (up to 4000 mAh g^{-1} for $Li_{21}Si_5$) [6]. Although Si is the most promising of next-generation anodes, it undergoes a large volume change during lithium insertion and extraction. This change results in pulverization of the Si and loss of electrical contact between the Si and the current-collector during lithiation and delithiation [7,8]. Thus, its capacity fades rapidly during cycling.

Attention has been placed on electrode materials in the multiphase form composed of two metal compounds [9]. The electrodes consisted of active and inactive metals. Inactive metals incapable of alloy formation with lithium include Mo, Fe, Ti and V [10]. Of these elements, Mo has both high electrical conductivity and a strong affinity for inactive materials and Si. An inactive metal matrix helps to reduce the mechanical disintegration of the multiphase electrode during cycling. The silicon powders become electrode material, and the composites usually show capacity from 600 to 800 mAh g^{-1} [11–13]. Another way to prepare composite electrodes is with thin film processes such as RF-magnetron sputtering deposition and pulsed laser deposition [14,15]. We have attempted to confirm that a $SiMo_x$-alloy thin film prepared by sputtering has potential for use as the anode in Li-ion batteries.

In this study, the electrochemical properties of $SiMo_x$-alloy electrodes are investigated in an attempt to overcome the problems of the single-phase Si electrode. The electrochemical performance of Si-based alloy electrodes is examined and discussed in relation to their microstructure and surface changes.

2. Experiment

Si and $SiMo_x$-alloy electrodes were deposited on electrolytically deposited Cu foil. If Cu is deposited electrolytically on a large copper roll in an aqueous bath containing a high concentration of $CuSO_4$,

* Corresponding author. Tel.: +82 2 2220 0386; fax: +82 2 2298 2850.
E-mail address: jwpark@hanyang.ac.kr (J.-W. Park).

0378-7753/$ – see front matter © 2009 Elsevier B.V. All rights reserved.
doi:10.1016/j.jpowsour.2009.05.047

the roughness of the resulting film can be controlled by the process conditions. Such a procedure was established by Iljin-copper Co. Ltd., who provided a roughened Cu foil. A $NaOH/H_2O = 1/100$ (v/v) solution was used to remove natural oxides from the surface of the Cu foil. Next, the cleaning solution was removed by annealing in a vacuum chamber (at 1.0×10^{-6} Torr) at 200 °C for 10 min. Finally, the chamber was cooled to room temperature.

The Si and $SiMo_x$-alloy electrodes were deposited on the roughened Cu foil with an arithmetic mean roughness (Ra) of 0.5 μm (around 18 μm thick) by radio-frequency magnetron sputtering from Si and Mo targets with 3 in. diameters (purchased from Kojundo Chemical Laboratory, Co., Ltd., Japan) at 99.9% purity. The chamber was evacuated down to 1.0×10^{-6} Torr as a base pressure, and a working pressure of 5 mTorr was maintained with Ar gas. The Si and $SiMo_x$-alloy electrodes were deposited with a constant power density of 5.48 W cm^{-2} on the Si target, and power densities of 0.44, 0.88, and 1.75 W cm^{-2} on the molybdenum target. The deposition time was 2 h, and the thickness of the electrode was about 4 μm.

The Si and $SiMo_x$-alloy electrodes were structurally characterized by means of X-ray diffraction (XRD) with a Rigaku, D. MAX2500 diffractometer using Cu K_α radiation (λ = 1.5418 Å), with a selected-area electron diffraction (SAED) pattern, and by using Raman spectroscopy (T64000, ISA Jobin-Y von). The Raman spectra were collected at room temperature, using the 514.4 nm line of an argon laser and a 50× magnification microscope on a small selected-area (about 2 μm^2) of the sample surface. Laser power was kept at about 2 mW.

The surface morphologies and topologies of the electrodes were measured using field-emission scanning electron microscopy (FESEM, JES 6340F, Jeol). X-ray photoelectron spectroscopy (XPS, ESCALAB 220i, THERMO VG SCOENTIFIC) with Al K_α radiation (1486.6 eV) was used to analyze the chemical bonding and the relative changes in the valence states of the silicon and the molybdenum ions. The spectra were calibrated with the carbon 1s line of a hydrocarbon located at 284.8 eV.

To evaluate the electrochemical properties of the electrodes, 1 M $LiPF_6$/ethylene carbonate (EC) and dimethyl carbonate (DMC), 1:1 in volume (Techno Semichem, Co., Ltd.) and lithium metal (100 μm thickness, Sigma–Aldrich, Co., Ltd.) was used as the electrolyte and lithium metal as the counter electrode. All three layers, including the Si electrode, the separator and the lithium metal, were stacked in a coin-type cell (CR2032, Hosen Co., Ltd., Japan) in an argon filled glove-box.

Galvanostatic charge–discharge half-cell tests were performed with a cycle tester (WBCS3000, Won a tech, Co. Ltd., Korea) at a constant current of 714 μA cm^{-2} (C/5 rate, C being defined as $1Li^+$ ion exchanged in 1 h) to a voltage cut-off at 1.0/0.01 V versus Li/Li^+. The cell was operated between the initial open-circuit voltage (OCV) and 0.01 V versus Li^+/Li, then between 0.01 and 1.0 V after the first cycle. To obtain the cyclic voltammogram, the scan rate was set at 0.01 mV s^{-1} in the same experimental system and voltage range. Charging and discharging of the cell relate to lithium extraction from and insertion into an active host, respectively. The electrode capacity was calculated according to the weight of the active material. The impedance spectrum of each coin cell was taken. The cell was allowed to equilibrate for 30 min before each measurement that was performed with a Zahner Elecktrik IM6 impedance analyzer over the frequency range from 1 MHz to 5 mHz at an amplitude of 10 mVrms.

3. Results and discussion

The four Si and $SiMo_x$-alloy electrodes had different thicknesses and weights depending on their Mo concentrations as determined by chemical analysis (Table 1). The samples were assigned a composition ratio according to the atomic percentages. The X-ray diffraction patterns of the as-deposited Si and $SiMo_x$-alloy electrodes are presented in Fig. 1. The three diffraction peaks from the copper foil were observed at 2θ positions of about 43.29°, 50.43° and 74.13° (JCDPDS 03-1005). There were no peaks related to crystalline Si, Mo or a $SiMo_x$-alloy. This implies that RF-sputtered films may have an amorphous structure.

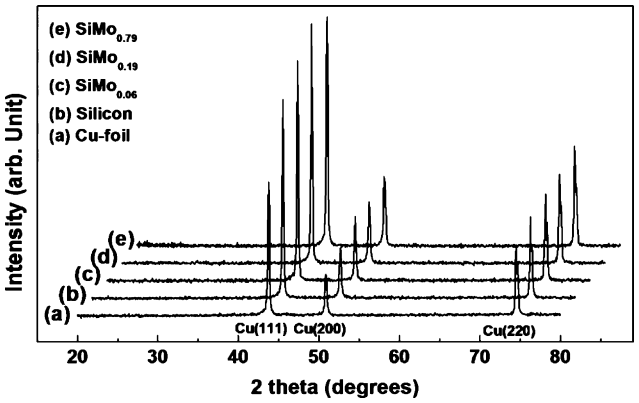

Fig. 1. XRD patterns of (a) Cu foil, (b) Si, (c) $SiMo_{0.06}$, (d) $SiMo_{0.19}$ and (e) $SiMo_{0.79}$ electrode deposited rough Cu foil.

Ex situ Raman spectroscopy was used to obtain structural information on the electrodes. The Raman spectra for the Si and $SiMo_{0.79}$-alloy electrodes are given in Fig. 2. It has been reported that the Raman peak of crystalline silicon can be observed at 520 cm^{-1} [16]. The deposited material prepared in this study is identified as amorphous Si because Raman spectroscopy detects the substantial presence of a peak around 480 cm^{-1} corresponding to an amorphous region and the absence of a peak around 520 cm^{-1} which characterizes a crystalline region. The amorphous component can be recognized in the spectra of both silicon and $SiMo_{0.79}$-alloy electrodes. The peaks corresponding to the silicon region in Fig. 2 were separated. The peaks around 430 and 460 cm^{-1} are related to the bonding of the silicon–molybdenum and the silicon oxide, respectively. This information can be used to study the molybdenum silicide thin film, as reported by Srinivas and Vankar, for example [17].

The TEM analysis was performed to analyze the electrodeposited copper foil and active material interface and reconfirm the structure of the electrodes. The cross-sectional TEM image of the deposited film presented in Fig. 3 reveals that the as-deposited Si–Mo film is composed of amorphous and some nano-crystalline phases. The inset shows the selected-area electron diffraction (SAED) pattern

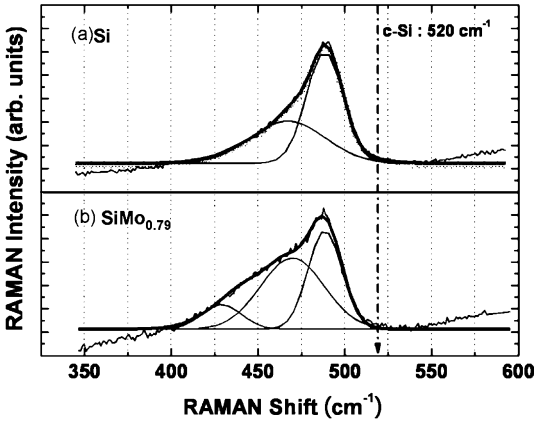

Fig. 2. Raman spectra of as-deposited (a) Si and (b) $SiMo_{0.79}$ electrode.

Table 1
Summary of physical properties of Si and $SiMo_x$-alloy electrodes.

Sample	At.% Si	At.% Mo	Wt.% Si	Wt.% Mo	Silicon mass (μg)	Molybdenum mass (μg)	Electrode thickness (μm)
Si	100	0	100	0	1530.40	0	3.0
$SiMo_{0.06}$	94.34	5.64	86.27	13.73	1530.40	243.52	3.1
$SiMo_{0.19}$	84.04	15.96	60.37	39.63	1530.40	999.62	3.45
$SiMo_{0.79}$	55.86	44.14	26.96	73.04	1530.40	4145.03	4.77

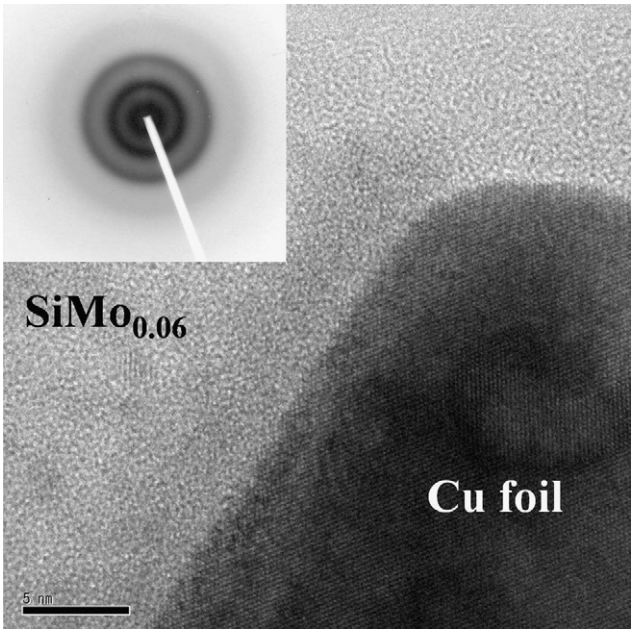

Fig. 3. TEM image and corresponding SAED pattern (inset of Fig. 2) of as-deposited $SiMo_{0.06}$ electrode prepared by RF-magnetron sputtering.

taken from the deposited film. The pattern consists of broad diffuse rings that are different from the clear rings/spots seen in the crystalline Si-phase. This proves that the deposited film has an amorphous structure. In general, the production of an amorphous structure is well suited to thin film techniques such as RF-sputtering or evaporation. The amorphous structure is usually more open than a well-crystallized one. It is recognized that an open structure prevents lattice expansion and provides many Li diffusion paths [18].

Fig. 4(a) and (b) shows SEM images of the surface of the electrolytically deposited copper foil, and of a film deposited on the electrodeposited copper foil. The surface of the copper foil has many irregularities (Fig. 4(a)) that increase the adhesion force between the deposited film and the foil. It is seen (Fig. 4(c)) that the surface morphology of the as-deposited film is also rough. The cross-section of the as-deposited film on the Cu foil is observed in Fig. 4(d). The thickness of the film is about 3 μm after 2 h of deposition and corresponds to a growth rate of about 25 nm per min. The surface morphology of the $SiMo_{0.79}$-alloy electrode on the Cu foil after 50 cycles of electrochemical measurements is presented in Fig. 4(e). Cracks form along the ravines after Li intercalation/deintercalation because of internal stress in the film that arises from volume changes. The cracked film has good adhesion to the Cu foil, and no pulverized particles are observed. In addition, there is no exfoliation of the columns from the copper foil.

Cyclic voltammetry (CV) analysis measured the electric potential over the region where the main reaction of an electrode occurs. Four CVs of the half-cell were measured between 0.01 and 1.0 V at a slow scan rate of 0.01 mV s^{-1}. The CV plots for the Si and $SiMo_x$-alloy electrodes are given in Fig. 5. In all plots, there are two sets of cathodic peaks, namely peaks at about 0.07 and 0.2 V, and anodic peaks at about 0.3 and 0.42 V. These peaks are attributed to potential-dependent reactions between different alloy phases.

The equilibrium potential values (mV versus Li/Li^+) for the solid system at room temperature [19] are 0.58 V ($Si/Li_{12}Si_7$), 0.52 V ($Li_{12}Si_7/Li_7Si_3$), 0.42 V ($Li_7Si_3/Li_{13}Si_4$), and 0.3 V ($Li_{13}Si_4/Li_{21}Si_5$). Due to the kinetic effect associated with the CV measurement, only two peaks, at 0.3 and 0.42 V, are present in the anodic scan. The potential difference between the anodic peaks and the cathodic peaks is due to polarization of the cell. The peaks observed dur-

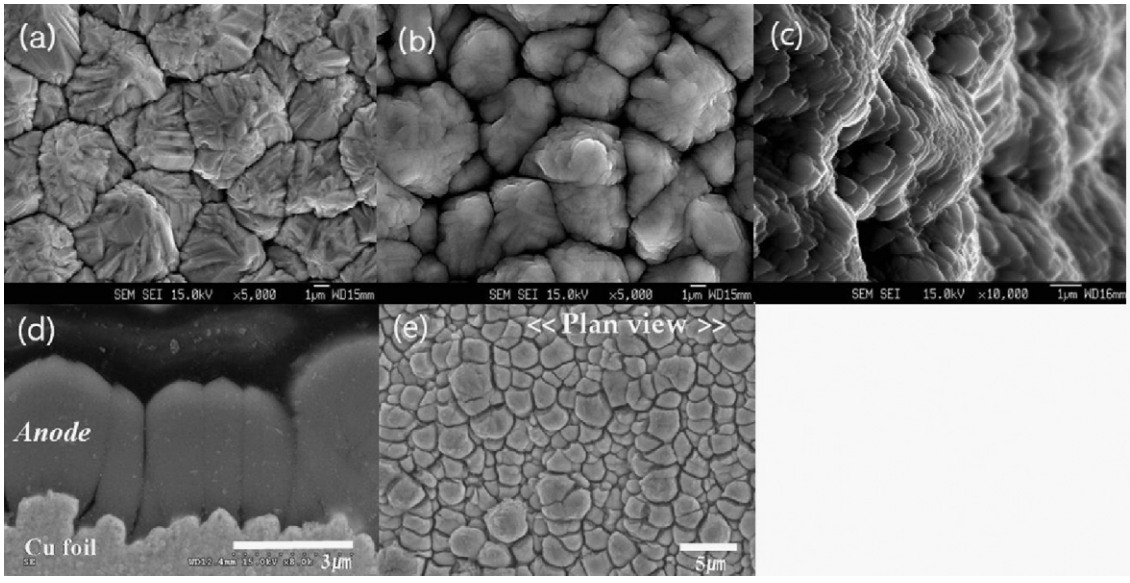

Fig. 4. SEM images of (a) electrodeposited Cu foil, (b) as-deposited $SiMo_{0.06}$ electrode, (c) 60° tilting image of (b), (d) cross-section image of (b) and (e) $SiMo_{0.79}$ electrode after 10 cycles.

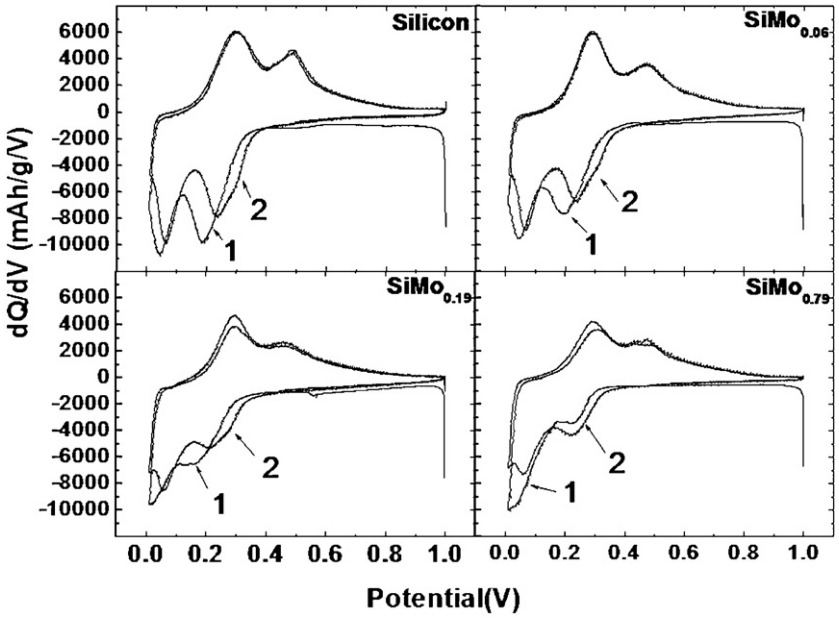

Fig. 5. Cyclic voltammetry (CV) plots of Si, $SiMo_{0.06}$, $SiMo_{0.19}$ and $SiMo_{0.79}$ electrode.

ing the second cycle are comparable with those of the first cycle in that they decrease significantly at 0.1/0.2 V and shift toward a higher potential. The irreversible reaction of the first cycle appears to be associated with the formation of a solid electrolyte interface (SEI) layer or a dangling bond, which is a phenomenon related to phase transformation [20]. Therefore, a significant reduction of the cathodic peak indicates that the irreversible reaction is suppressed by the maintenance of an equilibrium state in the second cycle. The area was not changed before the recharge. The results show an excellent initial capacity retention rate.

The capacity of the cell decreases with the formation of silicide generated during the bonding of the silicon and inactive material [21]. Therefore, the capacity changes with change in the ratio of the inactive material. Fig. 6 shows the voltage profiles of the Si and $SiMo_x$-alloy electrodes as a function of cycle number. The discharge capacities of the Si, $SiMo_{0.06}$, $SiMo_{0.19}$, and $SiMo_{0.79}$ electrodes are about 2200, 2000, 1800 and 1500 mAh g^{-1}. The Si electrode in Fig. 6(a) maintains the discharge capacity given on the first cycle until about the 35th cycle. By contrast, electrodes containing $SiMo_{0.06}$ in Fig. 6(b), $SiMo_{0.19}$ in Fig. 6(c), and $SiMo_{0.79}$ in Fig. 6(d), maintain the initial discharge capacity until about the 40, 45 and 60th cycles. During lithium insertion into the alloy electrodes, Si acts as an active center and reacts with Li to form amorphous Li_xSi alloys. The Si–Mo bonding in the electrode plays the role of a matrix in an inertial phase, which can buffer Si volume expansion and facilitate charge transfer among Si atoms.

A constant-current test was conducted to measure the charge and discharge characteristics of each electrode. Fig. 7 shows the discharge capacities of the Si and the $SiMo_x$-alloy electrodes as a function of cycle number. The cells were cycled between 0.01 and

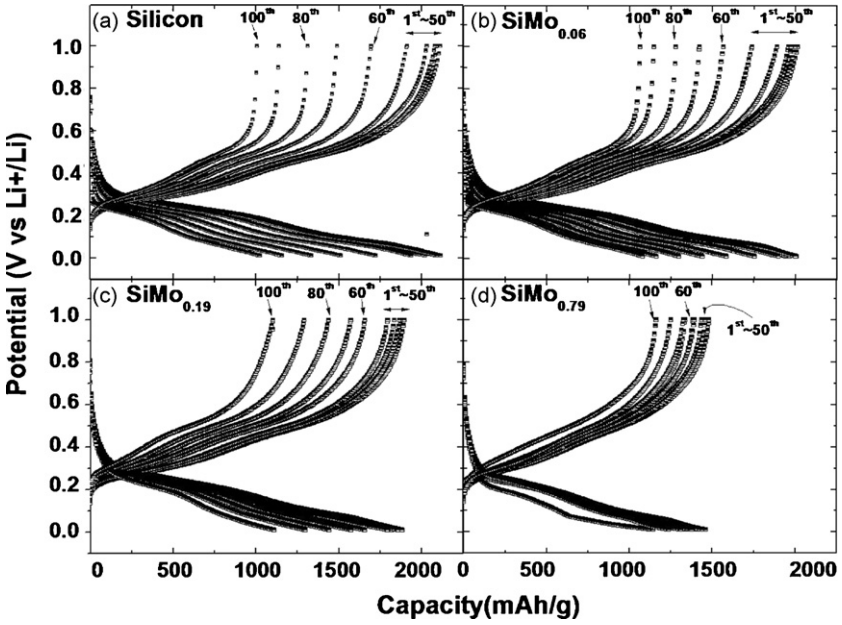

Fig. 6. Constant-current charge–discharge curves of Li for the as-deposited (a) Si, (b) $SiMo_{0.06}$, (c) $SiMo_{0.19}$ and (d) $SiMo_{0.79}$ electrode.

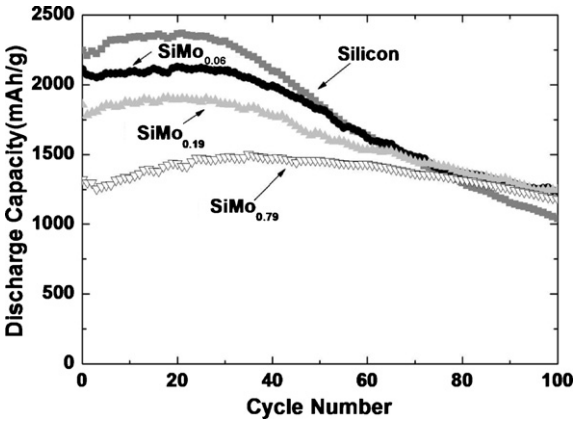

Fig. 7. Cycle performances of Si electrode and $SiMo_x$-alloy electrodes at various compositions: (a) Si, (b) $SiMo_{0.06}$, (c) $SiMo_{0.19}$ and (d) $SiMo_{0.79}$ electrode. Voltage window and current density were 0.01–1.0 V and 714 μAh g^{-1}.

1.0 V versus Li/Li^+ at a current density of 714 μA cm^{-2}. A high initial discharge capacity of 2200 mAh g^{-1} is obtained for the Si electrode. However, the reversible capacity of the electrode is continuously degraded up to 30 cycles, and the electrode gives a capacity of only about 1000 mAh g^{-1} after 100 cycles. For the $SiMo_{0.79}$ electrode, the initial discharge capacity is 1319 mAh g^{-1}, and its capacity is maintained at over 1180 mAh g^{-1} for 100 cycles. These results show that the $SiMo_{0.79}$ electrode has a much higher coulombic efficiency and better cycle retention than the Si electrode.

In the case of $SiMo_{0.79}$, while a cycling is progressing, there is a period during which the capacity increases slightly, which contributes to the recharging procedure. This occurs during the cycle in which the lithium caught within the electrode in which it acted in the first cycle as the irreversible capacity is stabilized. A sharp reduction in capacity does not occur in all $SiMo_x$-alloy electrodes. The Si and Mo comprise stable compounds and form a deactivation structure for which the capacity is stable.

Measurements were taken with ex situ XRD after finishing the electrochemistry tests of the $SiMo_x$-alloy electrodes. The angle and plane corresponding to each phase is indicated on the graph corresponding to the XRD peak. Both the pristine sample and the 100-cycle tested sample of each electrode were compared. After 100 cycles (Fig. 8), a small crystalline Si peak is generated by the pristine Si electrode, which has an amorphous structure, but the peak indicating crystalline Si disappears in Fig. 8(b)–(d) for the $SiMo_x$-alloy electrode. Notice that a Mo-silicide peak appears. This shows that a crystalline silicide is formed within the electrode. The peak appears when the silicide formed by the amorphous structure partially changes to a crystalline structure during cycling. The Si–Mo gives a buffer agent action that is stronger than the coherence of Si–Si and thereby controls the lithium-ion reaction and mitigates the volume expansion of Si.

Table 2
Abundance ratios in Si 2p spectra of the Si and $SiMo_{0.06}$, $SiMo_{0.19}$, and $SiMo_{0.79}$-alloy electrodes.

Sample	(2p) Metal silicon	(2p) Silicate	(2p) Silicide
Si	58.2%	41.8%	
$SiMo_{0.06}$	52.6%	11%	36.4%
$SiMo_{0.19}$	43.35%	20%	36.65%
$SiMo_{0.79}$	21.94%	17.85% (silicate or silicide) + 60.21% (silicide)	

The reason that $SiMo_x$-alloy electrodes have good electrochemical properties is found in the XPS spectra in Fig. 9. XPS spectrum can show which bonds exist in the electrode (Si–Si, Si–O, or Si–Mo), and which bond is the major. Each spectrum was fitted with a Gaussian peak and given an index [22]. The abundance ratios in the Si 2p spectra are shown in Table 2. A large change in the abundance of the silicon oxide (silicate) is not shown by the silicon 2p (Si: 41.8%, $SiMo_{0.06}$: 11%, $SiMo_{0.19}$: 20%, $SiMo_{0.79}$: <17.85%). With increased molybdenum concentration, however, the abundance ratios of metal silicon 2p (Si: 58.2%, $SiMo_{0.06}$: 52.6%, $SiMo_{0.19}$: 43.35%, $SiMo_{0.79}$: 21.94%) decrease and the abundance ratios of silicide (Si: 0%, $SiMo_{0.06}$: 36.4%, $SiMo_{0.19}$: 36.65%, the $SiMo_{0.79}$: >60.21%) increase. This confirms that a silicide is formed in the $SiMo_x$-alloy electrodes.

In the $SiMo_x$-alloy electrodes, the affinity between the Si and molybdenum is strong and allows a silicide to form [23]. As the volume of silicide is increased, the quantity of the active material is decreased. Consequently, the added molybdenum should be

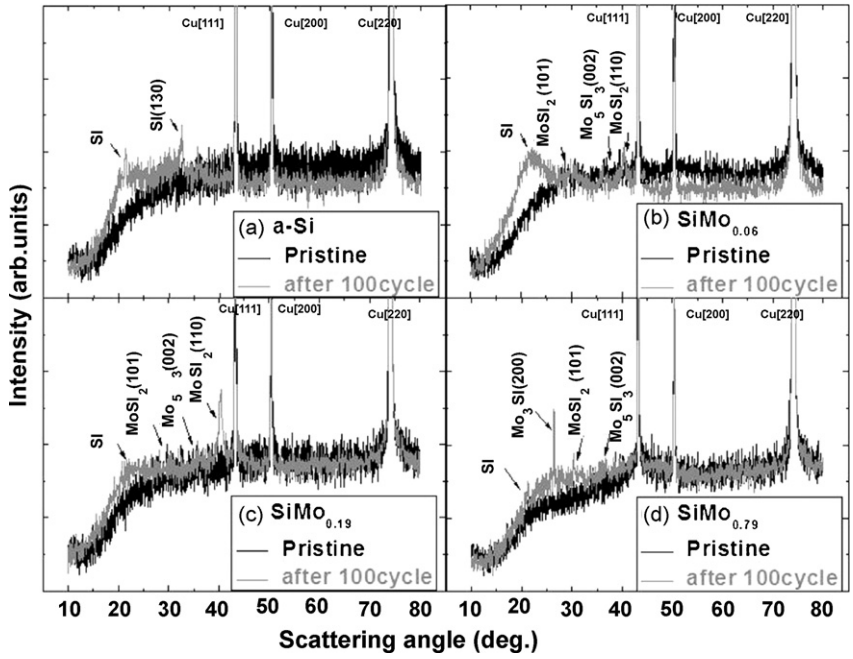

Fig. 8. XRD patterns of Si and $SiMo_x$-alloy electrodes after 100 cycles: (a) Si, (b) $SiMo_{0.06}$, (c) $SiMo_{0.19}$ and (d) $SiMo_{0.79}$ electrode.

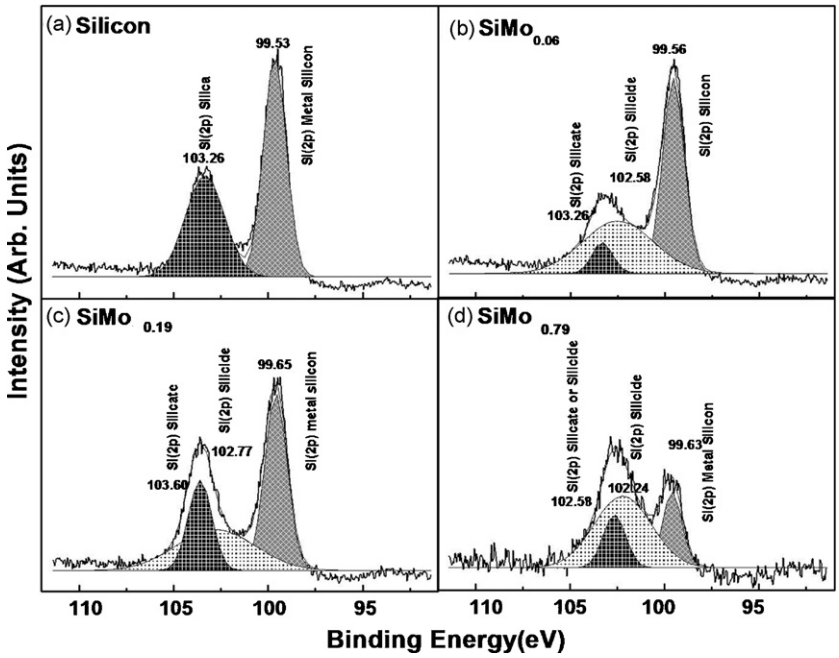

Fig. 9. XPS spectra of silicon 2p peak of $SiMo_x$-alloy electrodes at various compositions: (a) Si, (b) $SiMo_{0.06}$, (c) $SiMo_{0.19}$ and (d) $SiMo_{0.79}$ electrodes.

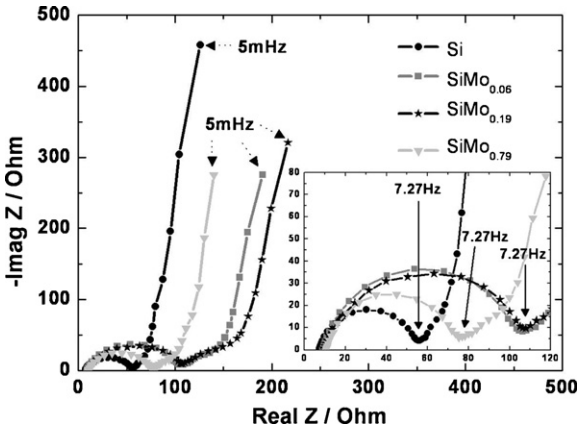

Fig. 10. Impedance spectra of Li/$SiMo_x$ cells in charged state to 1.0 V after fifth cycle.

minimized whereas the active material should be maximized. An adequate amount of silicide is important for the maintenance of a stable charge and discharge cycle.

The electrodes containing molybdenum have a low initial discharge voltage but a high capacity retention. Molybdenum silicide consisting of Si and Mo has a very high melting point and excellent mechanical strength [24,25]. However, it raises the resistance value of the total cell because the electric resistivity of molybdenum silicide is higher than that of Si and Mo. Molybdenum silicide has a much higher electric resistivity (0.2 M Ω m) than 5.52×10^{-8} Ω m for molybdenum, and 1×10^{-3} Ω m for silicon [26–28]. The Nyquist plot is composed of a small semi-circle in the high-frequency range and a sloping line in the low-frequency range. The high-frequency small semi-circle, as clearly shown in the inset of Fig. 10, is attributed to the electrolyte|Si (or $SiMo_x$) interfacial resistance, while the inclined line corresponds to the lithium-ion diffusion process (Warburg impedance) within the electrode. The value of the parameters calculated from the impedance data during the discharge process are summarized in Table 3. It can be seen that Z_w and R_{ct} show the same trend. When the content of molybdenum is increase, Z_w and R_{ct} increase and then subsequently decrease. Usually, Z_w (Warburg impedance) is mainly related to the diffusion path within the electrode materials. With increase in the content of molybdenum, Z_w decreases gradually and then reaches 2.3769 Ω at $SiMo_{0.79}$. Also, D_{Li^+} (diffusion coefficient) decreases for molybdenum-containing sample and then subsequently increases when the content of molybdenum increases. This indicates that the diffusivity of Li^+ of these alloy materials is lower than silicon. However, $SiMo_{0.79}$ exhibited high Li^+ diffusion, which was almost similar to Si.

The above observations explain two characteristics of the molybdenum-containing electrodes. It helps capacity maintenance by forming a buffer of $MoSi_x$, and relieves the mechanical stress in the electrode. On the other hand, the electric conductivity of the electrode may be reduced because of the high resistance value of the molybdenum silicide. The effect of molybdenum can be improved through appropriate control of the molybdenum concentration.

From these results, it is concluded that two parameters seem to contribute most to the electric performance of Si-based alloy electrodes. First, good uniformity of the molybdenum dispersed in the electrodes is essential for increasing the performance of the electrode after cycling because molybdenum acts as an electrical

Table 3
a.c. impedance parameters (Ω) for Si and $SiMo_x$-alloy electrodes.

Sample	R_s (Ω)	C_{dl} (μF)	R_{ct} (Ω)	σ (Ω cm^2 s$^{-1/2}$)	Z_w (Ω)	D_{Li^+} ($\times 10^{-7}$ cm^2 s^{-1})
Si	7.28	75.334	50.434	8.2946	1.7356	7.096
$SiMo_{0.06}$	9.073	57.749	97.284	15.736	3.2927	3.74
$SiMo_{0.19}$	5.701	54.177	98.177	15.369	3.2159	3.83
$SiMo_{0.79}$	10.647	52.26	66.13	11.3598	2.3769	5.18

connector. Second, molybdenum acts as a mechanical buffer against electrode pulverization caused by a large volume expansion.

Further studies are necessary to delineate clearly the exact role of Mo-silicide during the lithium insertion and de-insertion process. Mo-silicide is capable of accommodating the volume expansion of Si during charge–discharge cycling and enhances the electronic conduction path. It is believed that an optimized concentration of molybdenum is important for the enhanced capacities and good cycleability of $SiMo_x$-alloy electrodes. Nevertheless, based on the above results, it can be concluded that the $SiMo_{0.79}$ electrode has higher performance than Si, $SiMo_{0.06}$ or $SiMo_{0.19}$ and is promising for use as anodes for application in Li-ion batteries.

4. Conclusions

$SiMo_x$-alloy electrodes have been successfully fabricated using co-sputtering and an electrolytic deposited Cu foil, and show improved cycle performance and capacity retention compared with Si electrodes. A $SiMo_{0.79}$ electrode exhibits good capacity retention at 714 $\mu A\,cm^{-2}$; 89.4% of its original capacity is retained after 100 cycles. It is concluded that expanding the contact area between the deposited film and the substrate helps the active material to accommodate volume changes. A crack induced in the electrodes is seen in SEM images. This crack affects the stress relaxation of the electrodes. Also, the metal atoms form Si–Mo bonds and a partially inactive matrix. These inactive sites reduced mechanical stress during cycles.

In this study, co-sputtered Si-based alloy electrodes give excellent electrochemical performance. The electrodes show promise as next-generation anodes for rechargeable lithium batteries.

Acknowledgements

This work was financially supported by KOSEF through the Research Center for Energy Conversion and Storage and the Future Energy Research Institute.

References

[1] M. Yoshio, H. Wand, K. Fukuda, T. Umeno, N. Dimov, Z. Ogumi, J. Electrochem. Soc. 149 (2002) A1598.
[2] P. Limthongkul, Y.I. Jang, N.J. Dudney, Y.M. Ching, Acta Mater. 5 (2003) 11103.
[3] H. Li, X. Huang, L. Chen, Z. Wu, Y. Liang, Electrochem. Solid State Lett. 2 (2003) 165.
[4] Z.S. Wen, J. Yang, B.F. Wang, K. Wang, Y. Liu, Electrochem. Commun. 5 (2003) 165.
[5] Z. Chen, L. Christensen, J.R. Dahn, Electrochem. Commun. 5 (2003) 919.
[6] Y. Liu, K. Hanai, K. Horikawa, N. Imanishi, A. Hirano, Y. Takeda, Mater. Chem. Phys. 89 (2005) 80.
[7] H. Kim, J. Choi, H.J. Sohn, T. Kang, J. Electrochem. Soc. 146 (1999) 4401.
[8] K.-L. Lee, J.-Y. Jung, S.-W. Lee, H.-S. Moon, J.-W. Park, J. Power Sources 130 (2004) 241.
[9] W.G. Moffat, Handbook of Binary Phase Diagrams, Genium Publishing Co., Schnectady, NY, 1990.
[10] N. Takao, I. Tanaka, H. Adachi, Intermetallics 4 (1996) S113.
[11] Y. Hanshmoto, N. Machida, T. Shigematsu, Solid State Ionics 175 (2004) 177.
[12] K. Hanai, Y. Liu, N. Imanishi, A. Hirano, M. Matsumura, T. Ichikawa, Y. Takeda, J. Power Sources 146 (2005) 156.
[13] M.-S. Park, Y.-J. Lee, S. Rajendran, M.-S. Song, H.-S. Kim, J.-Y. Lee, Electrochim. Acta 50 (2005) 5561.
[14] J.-K. Ahn, S.-G. Yoon, Electrochim. Acta 50 (2004) 371.
[15] T. Ishihara, M. Nakasu, M. Yoshio, H. Nishiguchi, Y. Takita, J. Power Sources 146 (2005) 161.
[16] M. Birkholz, B. Selle, W. Fuhs, S. Chrestiansen, H.P. Strunk, R. Reich, Phys. Rev. B 64 (2001) 085402.
[17] G. Srinivas, V.D. Vankar, Mater. Lett. 30 (1997) 209–215.
[18] T. Motooka, O.W. Holland, Appl. Phys. Lett. 58 (1991) 2360.
[19] W.J. Weydanz, M.W. Mehrens, R.A. Huggins, J. Power Sources 81–82 (1999) 237.
[20] H. Li, X. Huang, L. Chen, Z. Wu, Y. Liang, Electrochem. Solid-State Lett. 2 (1999) 547.
[21] M.D. Fleischauer, J.M. Topple, J.R. Dahn, J. Electrochem. Soc. 8 (2005) A137.
[22] J.F. Moulder, W.F. Strickle, P.E. Sobol, K.D. Bomben, Handbook of X-ray Photoelectron Spectroscopy, Perkin-Elmer Co., Minnesota, 1992, p. 54.
[23] R.S. Rastogi, V.D. Vankar, K.L. Chopra, J. Vac. Sci. Technol. A 10 (1992) 2822.
[24] S.I. Kurganskii, N.S. Pereslavtseva, E.V. Levitskaya, Yu.A. Yurakov, Phys. Stat. Sol. (b) 233 (2) (2002) 306–311.
[25] M. Herranen, A.D. Bauer, J.O. Carlsson, R.F. Bunshah, Surf. Coat. Technol. 96 (1997) 245–254.
[26] The MEMS material database, in: J.F. Shackelford, W. Alexander (Eds.), CRC Materials Science and Engineering Handbook, 3rd edition, 2000, p. 567.
[27] D.R. Lide (Ed.), CRC Handbook of Chemistry and Physics, 81st edition, CRC Press, Boca Raton, FL, 2000, pp. 12–46.
[28] L.A. Hall, Survey of Electrical Resistivity Measurements on 16 Pure Metals in the Temperature Range 0 to 273K, NBS Technical Note 365, U.S. Superintendent of Documents, 1968.